VIP Electrocatalysis Very Important Paper

DOI: 10.1002/ange.201406281

Core/Shell Au/MnO Nanoparticles Prepared Through Controlled Oxidation of AuMn as an Electrocatalyst for Sensitive H_2O_2 Detection**

*Huiyuan Zhu, Aruna Sigdel, Sen Zhang, Dong Su, Zheng Xi, Qing Li, and Shouheng Sun**

Abstract: *Monodisperse 5 nm AuMn nanoparticles were synthesized by hydride reduction of manganese acetylacetonate in the presence of Au nanoparticles. The alloy was formed through fast Mn diffusion into the Au structure. The AuMn nanoparticles were converted to Au-MnO composite particles through air annealing at 170 °C. These Au-MnO particles, especially the core/shell Au/MnO nanoparticles, were active for the electrochemical reduction of H_2O_2, with a detection limit reaching 8 nM. This highly sensitive electrochemical sensor based on the Au/MnO nanoparticles was used to monitor H_2O_2 concentrations released from living cells, from which tumorigenic cells were discovered to release higher levels of H_2O_2 than the non-tumorigenic cells.*

Hydrogen peroxide is an important reactive oxygen species generated in cells through oxygen metabolism and is actively involved in cell signaling and cell growth. However, the uncontrolled overproduction of H_2O_2 can cause detrimental oxidation of biomolecules and lead to aging, cancer, and other diseases.[1] Therefore, the ability to monitor the H_2O_2 levels associated with different cells is considered an important step towards understanding the pathological, physiological, and biomedical function of H_2O_2. Conventionally, H_2O_2 concentrations are measured by assays based on H_2O_2 reduction catalyzed by horseradish peroxidase (HRP).[2] Alternatively, HRP-catalyzed H_2O_2 reduction can be detected by electrochemical methods.[3,4] To improve detection sensitivity, HRP is often anchored on the surface of gold (Au) nanoparticles (NPs) that have been predeposited onto the electrode to enrich HRP around the electrode surface.[5] Despite the high sensitivity and selectivity achieved, this enzyme-based sensor is of limited use owing to the complications associated with HRP purification, immobilization, and protection from denaturing. Recently, metal and metal oxide NPs that actively catalyze H_2O_2 reduction have been studied as enzyme-mimicking sensors to detect H_2O_2 in various environments.[6,7] Further studies have indicated that the detection sensitivity can be improved by using composite NPs such as dumbbell-like Au-Fe_3O_4 or PtPd-Fe_3O_4 NPs.[8,9] Specifically, PtPd-Fe_3O_4 NPs can detect H_2O_2 at nanomolar (nM) concentrations and can be applied to monitoring H_2O_2 released from RAW 264.7 cells (a mouse leukemia monocyte macrophage cell line).[9]

Herein, we report new core/shell structured Au/MnO NPs as a sensitive catalyst for the electrochemical detection of H_2O_2 with nM detection sensitivity, which is suitable for monitoring and quantifying the H_2O_2 released from cells. Metal oxide, especially Mn oxide NPs have been explored as biocompatible and enzyme-mimicking catalysts for H_2O_2 detection.[7b–f] However, these oxide NPs are generally not as active as Pt-based NPs in catalyzing the electrochemical reduction of H_2O_2 because of their poor electron conductivity. One strategy to improve the detection sensitivity is to couple the Mn-O with metallic NPs so that the synergistic effect can be applied to control both electron conductivity and catalytic activity. Among the common metal NPs studied, Au NPs come out as the best choice because Au is highly conductive and catalytically active for H_2O_2 reduction.[5,6a] More importantly, Au NPs are considered biocompatible.[5,10] We developed a unique approach to composite Au-MnO NPs by first preparing AuMn alloy NPs followed by air oxidation. We found that by controlling the AuMn composition, Au-MnO NPs with different morphologies could be obtained, as illustrated in Figure 1. These composite NPs were all active catalysts for the electrochemical reduction of H_2O_2 and the core/shell Au/MnO NPs showed the best activity, with an H_2O_2 detection limit reaching 8 nM. This high detection sensitivity allowed the quantification of H_2O_2 concentrations released from non-tumorigenic and tumorigenic cells.

To synthesize composite Au-MnO NPs, especially core/shell Au/MnO NPs, we tested the direct coating of MnO onto Au NPs through the decomposition of $Mn(acac)_2$ (acac = acetylacetonate) in the presence of Au NPs, but this approach failed. We also attempted to prepare Au/MnO through the oxidation of core/shell Au/Mn NPs. However, Mn prepared from the reduction of $Mn(acac)_2$ could not form a stable shell on the existing Au NPs. Rather, it diffused easily into the Au

[*] H. Zhu,[+] A. Sigdel,[+] Dr. S. Zhang,[$] [+] Z. Xi, Dr. Q. Li, Prof. S. Sun
Department of Chemistry, Brown University
Providence, RI 02912 (USA)
E-mail: ssun@brown.edu
Dr. D. Su
Center for Functional Nanomaterials
Brookhaven National Laboratory, Upton, NY 11973 (USA)
[$] Current address: Department of Chemistry
University of Pennsylvania, Philadelphia, PA 19104 (USA)
[+] These authors contributed equally to this work.

[**] Supported by the U.S. Army Research Laboratory and the U.S. Army Research Office under the Multi University Research Initiative (MURI, grant number W911NF-11-1-0353) on "Stress-Controlled Catalysis via Engineered Nanostructures". Electron microscopy work carried out at the Center for Functional Nanomaterials, Brookhaven National Laboratory was supported by the U.S. Department of Energy, Office of Basic Energy Sciences under Contract No. DE-AC02-98CH10886. We thank Dr. L. Chen of the Department of Polymer Science and Engineering, University of Massachusetts-Amherst for collecting XPS data.

Supporting information for this article is available on the WWW under http://dx.doi.org/10.1002/anie.201406281.

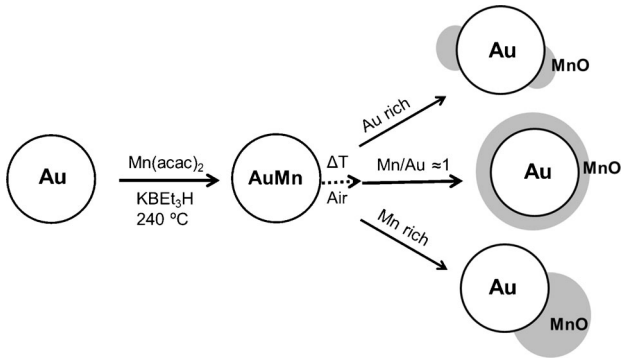

Figure 1. A schematic illustration of the controlled synthesis of Au-MnO composite NPs.

matrix, thereby resulting in an AuMn solid solution (Figure 1). Consequently, AuMn alloy NPs were readily synthesized. In a typical synthesis, 5 nm Au NPs were prepared as reported.[11] Then, in the presence of the Au NPs, $Mn(acac)_2$ was reduced by potassium triethylborohydride ($KBEt_3H$) to Mn that diffused quickly into the Au seeds to form a bimetallic alloy AuMn at 240 °C. The as-synthesized AuMn NPs were stabilized by oleylamine (OAm)and oleic acid (OAc) and could be dispersed in a nonpolar solvent such as hexane. The alloy NP compositions were controlled by the mass ratios of Au/$Mn(acac)_2$ and were measured by inductively coupled plasma atomic emission spectroscopy (ICP-AES). Figure 2 A and Figure S1 in the Supporting Information show typical transmission electron microscopy (TEM) images of the as-synthesized Au, $Au_{67}Mn_{33}$, $Au_{44}Mn_{56}$, and $Au_{35}Mn_{65}$ NPs. These NPs have an average diameter of 5 ± 0.2 nm for Au (Figure S1A), 5 ± 0.3 nm for $Au_{67}Mn_{33}$ (Figure 2 A), 5.5 ± 0.2 nm for $Au_{44}Mn_{56}$ (Figure S1B), and 5.7 ± 0.3 nm for $Au_{35}Mn_{65}$ (Figure S1C).

The formation of the AuMn alloy structure was characterized by high-resolution TEM (HRTEM), high-angle annular dark field (HAADF)-scanning transmission electron microscopy (STEM), and STEM electron energy-loss spectroscopy (STEM-EELS). As seen in the HRTEM image (Figure 2 B), the as-synthesized NPs display a pseudo-icosahedral shape with multi-twinned lattice fringes, a structure similar to that of premade polycrystalline Au NPs,[12] thus suggesting that the reaction conditions used in the current synthesis do not change the crystalline nature of the NPs. The HAADF-STEM image of the $Au_{67}Mn_{33}$ NPs (Figure 2 C) shows that all of the NPs give similar imaging intensity, thus indicating a uniform mix of Au and Mn within each NP. This is further confirmed by the EELS line-scan analysis of a typical $Au_{67}Mn_{33}$ NP (Figure 2 D), which shows a uniform Au/Mn distribution across the NP.

The solid solution structure of the AuMn NPs was further characterized by X-ray diffraction (XRD) and UV/Vis spectroscopy (Figure S2A,B). From the XRD, we can see that upon alloying Mn with the face-centered cubic (fcc) Au, the (111) peak shifts slightly to a higher angle without a change in peak width, thus indicating that the formation of the AuMn alloy reduces the structural lattice parameter but leads to no obvious change to the crystal structure. Furthermore, Au NPs dispersed in hexane show a plasmonic absorption at 522 nm. When Mn diffuses into the Au structure, the plasmonic absorption peak of the AuMn alloy NPs becomes broad and the intensity drops dramatically. An absorption at 535 nm was only observed from the Au-rich $Au_{67}Mn_{33}$ NPs. This plasmonic "quenching" in alloy NPs has previously been observed in other Au-based alloys, such as AuNi and AuPd,[13a,b] thus confirming that the AuMn NPs have a fcc-type solid solution structure.

To track the diffusion of Mn into the Au, we took aliquots from the system at different reaction stages for characterization. As shown in Figure S2C and Table S1 in the Supporting Information, from 130 °C to 240 °C, Mn is gradually alloyed with Au, and along with the increase of Mn in the alloy structure, the plasmonic absorption peak red-shifts and decreases in intensity. This result indicates that once Mn is deposited on the Au surface, it immediately diffuses into the Au lattice at the reaction temperature, thereby leaving no evidence of Mn coating of the Au NPs. Therefore, core/shell Au/Mn or Au/MnO could not be formed by using the synthetic conditions described.

To prepare Au-MnO composites, we first loaded the AuMn NPs onto Ketjen carbon (product denoted as C-AuMn) and annealed them in air at 170 °C to oxidize the Mn and remove the surfactant as reported.[11] TEM images of the C-$Au_{67}Mn_{33}$ and C-$Au_{44}Mn_{56}$ show no obvious NP morphology changes (Figure 3 A and Figure S3A), but the C-$Au_{35}Mn_{65}$ NPs look different (Figure S3B). The HRTEM image of a single annealed $Au_{35}Mn_{65}$ NP (Figure S3C) indicates a dumbbell-like structure as illustrated in Figure 1. HAADF-STEM 2D mapping and line scan allowed us to further characterize the structure changes during annealing. Figure 3 B and Figures S4A,B show the elemental mapping of the annealed AuMn NPs. In all three cases, the Mn phase segregates out onto the Au surface. Mn with stronger bonding to O_2 tends to diffuse out during the annealing process to form Mn oxide in a similar manner to what has been observed in AuNi and AuCu systems.[13a,c] Furthermore, this segregation

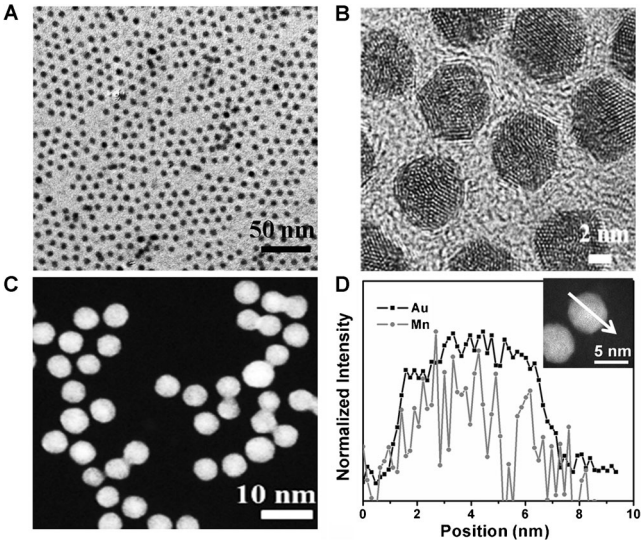

Figure 2. A) TEM image, B) HRTEM image, C) HAADF-STEM image, and D) STEM-EELS line scan of the as-synthesized $Au_{67}Mn_{33}$ NPs.

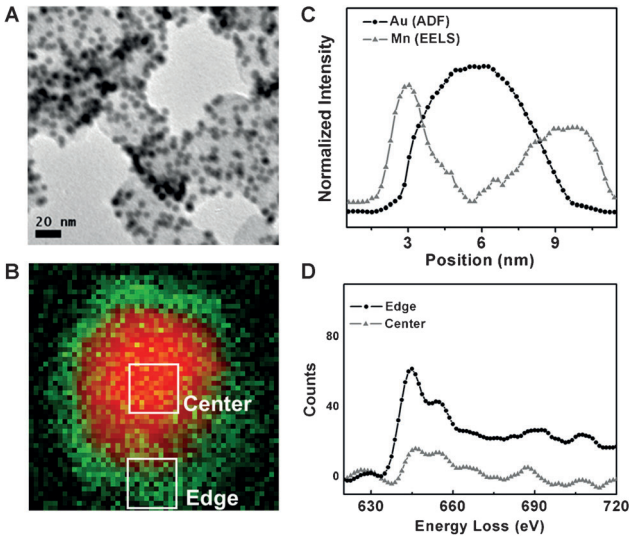

Figure 3. A) TEM image, B) STEM-EELS 2D mapping of C-$Au_{44}Mn_{56}$ after annealing, C) STEM-EELS line scan, and D) Mn L edges EELS spectra from the selected areas shown in (B).

was found to be composition dependent. The $Au_{67}Mn_{33}$ is converted to Au-MnO, with MnO forming isolated islands on the Au surface (Figure 1 and Figure S4A). If more Mn is present, as in the $Au_{35}Mn_{65}$, the new MnO phase self-aggregates on the Au surface to give a dumbbell-like structure (Figure 1 and Figure S4B). When the $Au_{44}Mn_{56}$ NPs are air-annealed, core/shell Au/MnO NPs are obtained (Figure 1 and Figure 3B). The core/shell structure was further confirmed by EELS line scan analysis (Figure 3C). This MnO shell is uniform as shown by the identical EELS (Figure 3D) recorded from the indicated regions in Figure 3B in the Mn L edges. The XRD patterns of the $Au_{44}Mn_{56}$ and Au/MnO NPs show no obvious peak change, thus suggesting that MnO in the Au/MnO has an amorphous structure (Figure S5A). X-ray photoelectron spectroscopy (XPS; Figure S5B,C) of the Au/MnO NPs shows a binding energy of 641.2 eV for Mn $2p_{3/2}$, which can be indexed to either Mn^{2+} (640.9 eV) or Mn^{3+} (641.9 eV).[14] Additionally, the difference in binding energy between Mn $2p_{1/2}$ and $2p_{3/2}$ was found to be 11.4 eV, a value close to the reported 11.6 eV for MnO (Figure S5C).[14a] This result, along with the well-known stability of MnO in Mn oxide chemistry and the air-annealing conditions we applied at 170 °C, leads us to believe that MnO is the oxide form most likely present in the core/shell structure.

To perform an electrochemical study of H_2O_2 reduction, a catalyst ink was prepared as reported.[15] 20 μL of the catalyst ink was drop-cast onto the glassy carbon electrode and dried under ambient conditions. Figure 4A shows the cyclic voltammograms (CVs) for the Au and Au/MnO NPs in N_2-saturated 0.1 M phosphate buffered saline (PBS) with and without 4 mM H_2O_2. The CVs for other Au-MnO NPs are given in Figure S6. All of the Au-MnO NPs exhibit higher reduction peak currents compared to pure Au NPs, with the core/shell Au/MnO NPs being the most active catalysts. The high activity of the Au/MnO NPs may be caused by their unique core/shell structure, where the maximal interfacial effect of MnO and Au occurs.

Chronoamperometry was applied to evaluate the sensitivity of the Au/MnO NPs for H_2O_2 detection. Figure 4B and Figure S7 present the current response of a glassy carbon (GC) electrode modified with Au/MnO NPs upon the addition of H_2O_2 at −0.28 V vs. Ag/AgCl. With the addition of 20 nM to up to 15.11 mM H_2O_2, the reduction current rapidly increases and reaches a steady state. Based on a signal-to-noise factor of 3 ($S/N = 3$), the detection limit can be calculated to be 8 nM. The calibration curve of current versus H_2O_2 concentration is shown in Figure 4C. The curve exhibits three different linear relationships in the ranges 20–100 nM ($R^2 = 0.9961$, sensitivity = 17850 μA mM^{-1} cm^{-2}), 100 nM–1111.1 μM ($R^2 = 0.9989$, with sensitivity = 208 μA mM^{-1} cm^{-2}), and 1111.1 μM–15.11 mM ($R^2 = 0.9973$, sensitivity = 530 μA mM^{-1} cm^{-2}), respectively. This may be caused by different reduction kinetics at different H_2O_2 concentrations. H_2O_2 reduction is dominated by H_2O_2 adsorption at extremely low H_2O_2 concentrations, whereas H_2O_2 activation becomes the rate-determining step when the H_2O_2 concentration is very high. In the middle region, H_2O_2 reduction is controlled by the combination of H_2O_2 adsorption and activation.

With high sensitivity achieved, the Au/MnO NPs can be used to detect the H_2O_2 released from living cells. H_2O_2 release was triggered by adding *N*-formylmethionyl leucyl phenylalanine (fMLP), which leads to H_2O_2 release that can resemble the oxidative metabolism most likely to be encountered in vivo.[7b,9] In the presence of MDA-MB-435S cells (human breast melanoma cells), HCT116 cells (human colorectal carcinoma cells), or M4A4 cells (human epithelial cells), the addition of 8 μM fMLP led to an immediate current response (Figure 4D). Without cells, no current response was recorded, thus suggesting that the current change is due to H_2O_2 being released from the living cells. We can further distinguish these cells by the current response. The current change for non-tumorigenic MDA-MB-435S cells (count: 0.7×10^6) is 0.3 μA, which corresponds to 12 pM H_2O_2 released per cell; however, the tumorigenic HCT116 (count: 2.5×10^6) and M4A4 (count: 2.4×10^6) cells give current changes of 2.5 μA and 3.3 μA, respectively, which correspond to 25 pM and 33 pM H_2O_2 released per cell. This result is consistent with the fact that tumorigenic cells tend to generate more H_2O_2 owing to their fast oxygen metabolism. This study demonstrates that our Au/MnO NP electrode presents a sensitive probe for extracellular H_2O_2 detection.

In summary, we have developed a new method for synthesizing AuMn alloy NPs through a seed-mediated atomic diffusion process. The morphology and composition of the as-synthesized AuMn NPs are well controlled. When annealed in air, these AuMn NPs are converted into composite Au-MnO or core/shell Au/MnO NPs depending on the Au/Mn composition ratios. These composite NPs, especially core/shell Au/MnO NPs, are active for the electrochemical reduction of H_2O_2 with a detection limit reaching 8 nM. They are highly efficient in distinguishing non-tumorigenic and tumorigenic cells through monitoring of the H_2O_2 levels released from these cells. These particles could be used as a sensitive probe for cancer detection.

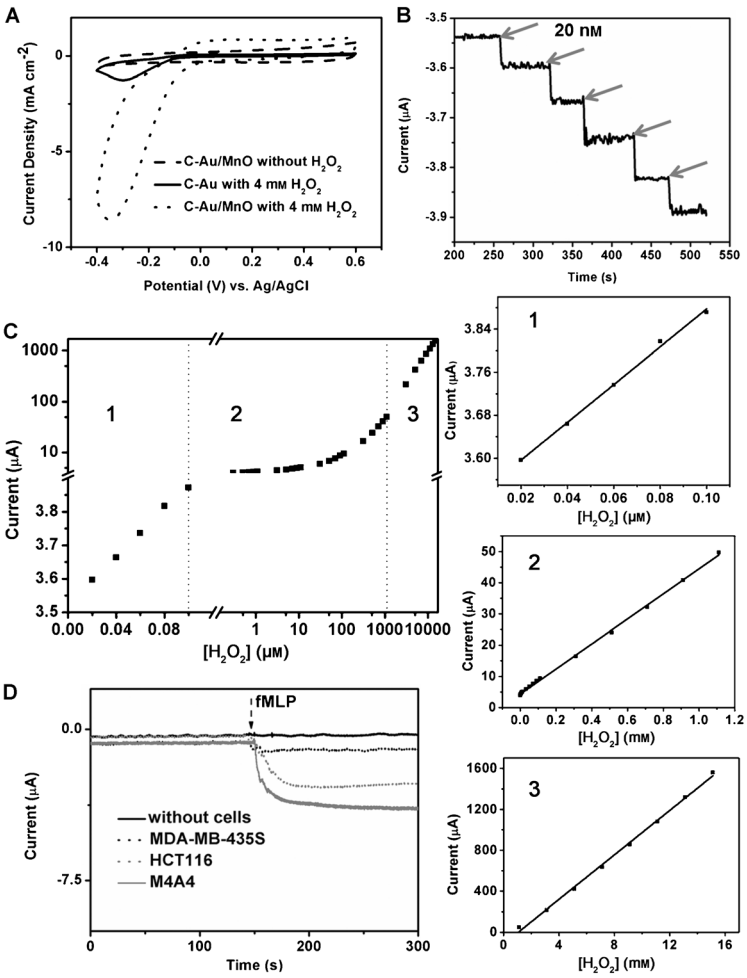

Figure 4. A) CVs of Au and Au/MnO NPs with or without the presence of 4 mM H_2O_2 in 0.1 M PBS. B) Current–time plot of the Au/MnO with successive additions of H_2O_2 from 20 nM (to a final concentration of 100 nM) in 0.1 M PBS at −0.28 V. C) Calibration curve of current vs. H_2O_2 concentration. The curve is split into three regions; 1, 2, and 3; which are plotted separately to clearly show the linear relationship between current and H_2O_2 concentration. D) Amperometric response of the Au/MnO modified electrode in the presence of no cells, MDA-MB-435S cells, HCT116 cells, or M4A4 cells for the detection of H_2O_2 release.

Experimental Section

Synthesis of $Au_{67}Mn_{33}$ NPs: 100 mg $Mn(acac)_2$ was mixed (by magnetic stirring) with 2.5 mL oleylamine (OAm) and 12 mL 1-octadecene (ODE) and heated to 110 °C for 30 min under a gentle flow of N_2 to remove the dissolved oxygen and moisture. 60 mg OAm-coated Au NPs in hexane dispersion were then added into the reaction system. After 5 min, 2 mL $KBEt_3H$ was added and the reaction mixture was heated to 240 °C at a rate of 4–5 °C min^{-1}. After 1 h, the reaction solution was air-cooled to room temperature. The solution was transferred into a 50 mL centrifuge tube, 3 mL OAm and 3 mL oleic acid (OAc) were added to the solution to further stabilize the as-synthesized NPs, and the mixed solution was left to stand for 12 h. The AuMn NPs were precipitated out by the addition of 35 mL isopropanol and centrifugation at 10000 rpm for 8 min, followed by ethanol wash and centrifugation (10000 rpm, 8 min). The AuMn NPs were further purified by dispersion in 20 mL hexane and centrifugation at 5000 rpm for 7 min to remove any undispersed impurities. The AuMn NPs were dispersed in hexane for further use.

Under the same reaction conditions, 150 mg $Mn(acac)_2$, 60 mg Au seeds, and 2.5 mL $KBEt_3H$ yielded $Au_{44}Mn_{56}$ NPs while 200 mg $Mn(acac)_2$, 60 mg Au seeds, and 3 mL $KBEt_3H$ produced $Au_{35}Mn_{65}$ NPs.

From AuMn to Au-MnO: The as-synthesized NPs, including both Au and AuMn NPs, were loaded on Ketjen-300J carbon (C) at a ratio of 4:6 (by weight) in 20 mL hexane by sonication for 1 h until the hexane solution turned clear. After washing with ethanol, the product was annealed in air at 170 °C overnight to remove the surfactant.[11,15b]

Cell Culture: All of the cells were incubated at 37 °C with 5% CO_2 in Dulbecco's Modified Eagle Medium (DMEM) with 10% fetal bovine serum (FBS) and 1% Penicillin-Streptomycin. Cells were grown up to 80% confluency. After washing with PBS twice, the cells were trypsinized and collected by centrifugation, and then redispersed in 2 mL 1 × PBS for further use.

Electrochemical Measurements: The NP-coated electrode was cleaned by scanning CV between 0.6 V to −0.4 V vs. Ag/AgCl 60 times. CVs were obtained by scanning between 0.6 V to −0.4 V vs. Ag/AgCl at a scan rate of 50 mv/s in N_2-saturated 0.1 M PBS without and with 4 mM H_2O_2 to evaluate the catalyst activity. The chronoamperometric test was applied at −0.28 V vs. Ag/AgCl. After the background current reached a steady-state, a successive addition of H_2O_2 starting from 20 nM was applied in the system to study the detection limit of the Au/MnO NPs.

Detection of H_2O_2 released from cells: After growing to 80% confluency, the cells were washed with PBS and counted by using a hemocytometer. 0.7×10^6, 2.4×10^6, 2.5×10^6 of MDA-MB-435S, M4A4, and HCT116 cells, respectively, were used and added into the 0.1 M PBS. The electrochemical system was deoxygenated under N_2. Current–time curves were recorded at −0.28 V vs. Ag/AgCl and after a background steady state current was obtained, 8 μM fMLP was added into the system and the corresponding current change was recorded.

Received: June 16, 2014
Published online: August 26, 2014

Keywords: gold · hydrogen peroxide · manganese · nanoparticles · sensors

[1] a) B. Halliwell, *J. Neurochem.* **1992**, *59*, 1609–1623; b) W. Dröge, H. M. Schipper, *Aging Cell* **2007**, *6*, 361–370; c) D. J. Rossi, C. H. M. Jamieson, I. L. Weissman, *Cell* **2008**, *132*, 681–696; d) E. A. L. Martins, R. Meneghini, *Biochem. J.* **1994**, *299*, 137–140.

[2] M. N. Tahir, R. Andre, J. K. Sahoo, F. D. Jochum, P. Theato, F. Natalio, R. Berger, R. Branscheid, U. Kolb, W. Tremel, *Nanoscale* **2011**, *3*, 3907–3914.

[3] a) P. Wu, Z. Cai, J. Chen, H. Zhang, C. Cai, *Biosens. Bioelectron.* **2011**, *26*, 4012–4017; b) M. Ali, M. N. Tahir, Z. Siwy, R. Neumann, W. Tremel, W. Ensinger, *Anal. Chem.* **2011**, *83*, 1673–1680.

[4] W. Chen, S. Cai, Q. Ren, W. Wen, Y. Zhao, *Analyst* **2012**, *137*, 49–58.

[5] a) L. Wang, E. Wang, *Electrochem. Commun.* **2004**, *6*, 225–229; b) F. Li, Y. Feng, Z. Wang, L. Yang, L. Zhou, B. Tang, *Biosens. Bioelectron.* **2010**, *25*, 2244–2248; c) J. Zhang, M. Oyama, *Electrochim. Acta* **2004**, *50*, 85–90.

[6] a) F. Meng, X. Yan, L. Liu, J. Gu, Z. Zou, *Electrochim. Acta* **2011**, *56*, 4657–4662; b) J. Yin, X. Qi, L. Yang, G. Hao, J. Li, J. Zhong, *Electrochim. Acta* **2011**, *56*, 3884–3889.

[7] a) H. Wang, X. Bo, J. Bai, L. Wang, L. Guo, *J. Electroanal. Chem.* **2011**, *662*, 281 – 287; b) F. Xiao, Y. Li, X. Zan, K. Liao, R. Xu, H. Duan, *Adv. Funct. Mater.* **2012**, *22*, 2487 – 2494; c) Y. Lin, X. Cui, L. Li, *Electrochem. Commun.* **2005**, *7*, 166 – 172; d) Y. Bai, H. Zhang, J. Xu, H. Chen, *J. Phys. Chem. C* **2008**, *112*, 18984 – 18990; e) C. E. Langley, B. Sljukic, C. E. Banks, R. G. Compton, *Anal. Sci.* **2007**, *23*, 165 – 170; f) Y. Bai, Y. Du, J. Xu, H. Chen, *Electrochem. Commun.* **2007**, *9*, 2611 – 2616.

[8] Y. Lee, M. A. Garcia, N. A. F. Huls, S. Sun, *Angew. Chem. Int. Ed.* **2010**, *49*, 1271 – 1274; *Angew. Chem.* **2010**, *122*, 1293 – 1296.

[9] X. Sun, S. Guo, Y. Liu, S. Sun, *Nano Lett.* **2012**, *12*, 4859 – 4863.

[10] C. Xu, J. Xie, D. Ho, C. Wang, N. Kohler, E. G. Walsh, J. R. Morgan, Y. E. Chin, S. Sun, *Angew. Chem. Int. Ed.* **2008**, *47*, 173 – 176; *Angew. Chem.* **2008**, *120*, 179 – 182.

[11] W. Zhu, R. Michalsky, O. Metin, H. Lv, S. Guo, C. J. Wright, X. Sun, A. A. Peterson, S. Sun, *J. Am. Chem. Soc.* **2013**, *135*, 16833 – 16836.

[12] a) W. Chen, R. Yu, L. Li, A. Wang, Q. Peng, Y. Li, *Angew. Chem. Int. Ed.* **2010**, *49*, 2917 – 2921; *Angew. Chem.* **2010**, *122*, 2979 – 2983; b) S. Peng, Y. Lee, C. Wang, H. Yin, S. Dai, S. Sun, *Nano Res.* **2008**, *1*, 229 – 234.

[13] a) S. Zhou, H. Yin, V. Schwartz, Z. Wu, D. Mullins, B. Eichhorn, S. H. Overbury, S. Dai, *ChemPhysChem* **2008**, *9*, 2475 – 2479; b) O. Metin, X. Sun, S. Sun, *Nanoscale* **2013**, *5*, 910 – 912; c) N. E. Motl, J. F. Bondi, R. E. Schaak, *Chem. Mater.* **2012**, *24*, 1552 – 1554.

[14] a) G. Xu, L. Zhang, C. Guo, L. Gu, X. Wang, P. Han, K. Zhang, C. Zhang, G. Cui, *Electrochim. Acta* **2012**, *85*, 345 – 351; b) H. W. Nesbitt, D. Banerjee, *Am. Mineral.* **1998**, *83*, 305 – 315.

[15] a) H. Zhu, S. Zhang, S. Guo, D. Su, S. Sun, *J. Am. Chem. Soc.* **2013**, *135*, 7130 – 7133; b) H. Zhu, S. Zhang, Y. Huang, L. Wu, S. Sun, *Nano Lett.* **2013**, *13*, 2947 – 2951.